Original Article

Journal of Intelligent Material Systems and Structures

Journal of Intelligent Material Systems and Structures
1–14

DOI: 10.1177/1045389X17704521
journals.sagepub.com/home/jim
SAGE

Design and integration sensitivity of a morphing trailing edge on a reference airfoil: The effect on high-altitude long-endurance aircraft performance

Pierluigi Della Vecchia[1], Salvatore Corcione[1], Rosario Pecora[1], Fabrizio Nicolosi[1], Ignazio Dimino[2] and Antonio Concilio[2]

Abstract

Trailing edge modification is one of the most effective ways to achieve camber variations. Usual flaps and aileron implement this concept and allow facing the different needs related to take-off, landing, and maneuver operations. The extension of this idea to meet other necessities, less dramatic in terms of geometry change yet useful a lot to increase the aircraft performance, moves toward the so-called morphing architectures, a compact version of the formers and inserted within the frame of the smart structures' design philosophy. Mechanic (whether compliant or kinematic), actuation and sensor systems, together with all the other devices necessary for its proper working, are embedded into the body envelope. After the successful experiences, gained inside the SARISTU (SmARt Intelligent Aircraft STrUctures) project where an adaptive trailing edge was developed with the aim of compensating the weight variations in a medium-size commercial aircraft (for instance, occurring during cruise), the team herein exploits the defined architecture in the wing of a typical airfoil, used on high-altitude long-endurance aircraft such as the Global Hawk. Among the peculiarities of this kind of aerial vehicle, there is the long endurance, in turn, associated with a massive fuel storage (approximately around 50% of the total weight). A segmented, finger-like, rib layout is considered to physically implement the transition from the baseline airfoil to the target configurations. This article deals with an extensive estimation of the possible benefits related to the implementation of this device on that class of planes. Parametric aerodynamic analyses are performed to evaluate the effects of different architectural layouts (in-plane geometry extension) and different shape envelopes (namely, the rotation boundaries). Finally, the expected improvements in the global high-altitude long-endurance aircraft performance are evaluated, following the implementation of the referred morphing device.

Keywords

Morphing structure, high-altitude long-endurance aircraft, aircraft performance

Introduction

Morphing is one of the most active research fields, currently. It deals with continuous modifications of the geometrical shape of a reference surface through actuator systems that are completely embedded into the structure. The reason behind this technology can be searched to the willingness of having more and more performant wings, in terms of aerodynamics or operational envelope. As presented, in fact, the fulfillment of this capability would open the door to many breakthrough improvements. For instance, it would allow avoiding any structural discontinuity in the command appliances, having no more nacelles to cover the massive mechanisms currently used to move flaps, slats, and the other flight control and maneuver devices (getting lightest and cleanest wings), introducing new aircraft capabilities by enlarging its operable degrees of freedom. As usual, however, a technology that envisages exceptional advantages also opens the window to many criticalities. An aerodynamic system with augmented degrees of freedom presents a complex response

[1]Aerospace Division, Department of Industrial Engineering, University of Naples "Federico II," Naples, Italy
[2]Adaptive Structures Division, Italian Aerospace Research Centre (CIRA), Capua, Italy

Corresponding author:
Pierluigi Della Vecchia, Aerospace Division, Department of Industrial Engineering, University of Naples "Federico II," via Claudio 21, 80125 Naples, Italy.
Email: pierluigi.dellavecchia@unina.it

that can lead to aeroelastic instabilities and then exalts the importance of a proper fluid–structural coupling design. More in general, the architectural complexity can have important impacts on safety, weight, costs, maintenance, and so on, mainly for the drastic increase in the number of parts, including the active elements. The availability of a pre-design tool, able to predict within a certain margin of uncertainty the expected benefits, is then necessary to properly address the design activities and evaluate the actual convenience of a particular architecture.

In a classical conceptual design, the aircraft geometry is typically optimized for a single flight segment (usually, cruise for a transport aircraft), compromising the performance at other conditions (Raymer, 2006). To overcome this limitation, discrete surfaces such as flaps and slats are deployed to modify the wing profile and adapt it to off-design flight phases. Bowman et al. (2007) evidenced how those devices can be intrinsically accounted as morphing systems, deployed to modify the wing shape and improve some targeted performance. The same authors showed that there is a crossover point for most applications where fuel drawbacks begin exceeding a possible morphing weight penalty. However, when the overall system performance and mission requirements are assessed, large shape change concepts can be a viable approach for some missions, particularly those that combine several and diverse requirements, for instance, in terms of speed, altitude, take-off, and landing. The adaptive wing would allow a given aircraft performing multiple missions and enable a single aircraft with multi-role capabilities, radically expanding its flight envelope (Barbarino et al., 2011). In that work, a comprehensive review of morphing aircraft is carried out. The authors addressed a systematic review of concepts, dividing them into sub-categories for fixed or rotary wing, planform, out-of-plane, and airfoil morphing and classifying motivations and results for each of the reported technologies. They also stated that there is an emerging interest in high-altitude long-endurance (HALE) aircraft that are designed to fly for several days. These planes have a larger portion of fuel weight (more than 50%), but they are designed to fly at a sole lift coefficient. When the aircraft weight decreases, the aircraft speed has to be reduced or the altitude has to be increased to maintain the optimal configuration. Moreover, such planes usually do not have good take-off and landing performance because they miss high lift devices. A morphing aircraft can modify its geometry continuously as a response to the changes in the flight conditions, to keep high performance levels throughout the mission. In the same way, the ability to change their shape enables morphing vehicles for facing multiple missions (Ajaj et al., 2016).

Usually, the approach to the morphing problem begins with the identification of a certain need by the manufacturer with reference to a specific product. In the case herein discussed, it deals with the increase in the range or the loitering performance improvement of a selected unmanned vehicle. Because the most obvious way is to act on the compensation of the weight following the fuel consumption, requiring in turn a different trim of the aerodynamic surfaces or a change in the flight conditions, a wing camber variation could represent the optimal answer. Such a property would simulate the availability of an airfoil portfolio along the defined mission. The immediate way to achieve a curvature modification is to act on the trailing edge, the less critical region of a wing structure. Different studies, spanning over a long time, did demonstrate that such operations could actually lead to important changes in the reference polar. The possibility of accessing to continuous deformations makes possible to think of a polar envelope (meant as the curve embedding all the possible polars) instead of a single polar for the considered airfoil. Many questions, however, arise, as for instance: how much should the modified trailing edge extend in chord and span? Are the allowable dimensions feasible to host a suitable mechanic system, integrating the actuators and the kinematics? Does the expected performance satisfy the expectations and offer a suitable margin for justifying weight, cost, and complexity increment? A first, preliminary response, still not ultimate, is necessary to address the engineering problem, correctly. Suitable tools and competences are necessary to accomplish this goal and attain a satisfactory answer. It could also permit rescheduling the planned investigations and show alternative paths. Nowadays, the interest has moved toward the application in small aircraft and unmanned aircraft vehicles (UAVs) due to a higher efficiency request and short time-to-deliver because of the reduced certification issues and qualification tests. This article deals with the design, integration, and sensitivity analyses of a morphing trailing edge on a selected HALE airfoil, finalized at the improvement of the general aircraft performance. The NASA low Reynolds number (LRN) 1015 profile was assumed as the reference starting point, properly designed for exhibiting minimum drag at high lift coefficient. It was employed on the long-endurance UAV RQ-4 Global Hawk, produced by Northrop Grumman. This airfoil was largely tested at the Transonic Wind Tunnel at NASA Ames Research Center. The experimental results at several Mach and Reynolds numbers can be found in the literature (Hicks and Cliff, 1991). In detail, its characteristics were measured at 0.20, 0.50, 0.55, and 0.60 M and at nominal 500,000, 1,000,000, and 2,000,000 Re. The experimented angles of attack ranged from around $-6.0°$ to $18.0°$.

To investigate the aerodynamic behavior of the LRN 1015, equipped with a morphing trailing edge, a discrete parametrization of its geometry was required. In fact, a numerical procedure uses coordinates or

control points to represent the airfoil geometry. In principle, each of them is a design variable to attain a desired shape, leading to a high number of independent parameters. To reduce the unknowns, several approaches may be considered. For instance, an interesting survey on parametrization techniques can be found in Samareh (1999). Most widely used procedures to fit airfoil shapes via interpolation are B-splines and Bezier curves (Derksen and Rogalsky, 2010; Drela, 1989; Fudenberg and Tirole, 1991). In the literature, analytical functions derived to represent families of profiles are also reported (Hicks and Henne, 1978). The PARSEC method, elaborated by Sobieczky (1997, 1998), has been widely used to represent and optimize aerodynamic geometries (Della Vecchia, 2013; Della Vecchia et al., 2014). Another technique used to parametrize aerodynamic shapes is based on the radial basic functions, well described by Fincham and Friswell (2015). Among the other methods, it is worth to cite Hicks–Henne (Hicks and Henne, 1978), Wagner (Ramamoorthy et al., 1969), Legendre (Hicks and Vanderplaats, 1975), Bernstein (Lane and Marshall, 2009), and NACA normal modes (Chang et al., 1995). They are based on polynomials representing a series of sinusoidal curves that are generated along a specified chord portion and operate by adding a sum of shape functions to certain airfoil geometry to generate a target form. All the above parametrization techniques could be implemented for the problem at hand. However, the technique based on polynomial functions could lead to non-feasible shapes (De Gaspari and Ricci, 2010). B-splines, non-uniform rational basis spline (NURBS), and so on could generate crossovers among neighboring points or lead to non-controlled geometries with negative impacts on their practical implementation. These drawbacks conduct, in turn, to difficulties in defining proper bounds for the design variables, in particular for the points that are close to the leading and the trailing edges. Such issues can be partly addressed by fixing the chord-wise coordinates of some control points in the affected regions. To ensure a smooth geometry and avoid crossovers between upper and lower surfaces, some geometric constraints can also be applied, limiting the design space that is explored by optimization methods (Wenbin, 2011). A rational parametrization was herein considered as the best way to assure the compliance of optimal aerodynamic solutions with structural and manufacturing requirements.

Several works have been focused on the aerodynamic analyses of two-dimensional (2D) morphed trailing edge, aiming at evaluating the action effects of this device on the aerodynamic coefficients. Kaul and Nguyen (2014) reported the numerical results of a study carried out on a generic commercial aircraft flap with a continuous camber variation, evidencing the drag reduction and the efficiency improvement. Lafountain et al. (2009) showed the design of a camber control system applied on a UAV aircraft, with the twofold purpose of improving its aerodynamic performance and its stealth capability. In fact, the movable surfaces' removal could significantly reduce its radar signature. The numerical and experimental validation of a morphing wing tip device concept was reported by Gabor et al. (2016), underlining the laminar flow extension and the relevant drag reduction benefits. Bolonkin and Gilyard (1999) estimated the advantages of developing a variable wing camber control system for transport aircraft, quantifying an improvement higher than 10% in non-standard flight conditions (at high lift coefficient) and around 1%–3% in cruise. They presented the lift-to-drag ratio improvement due to the deflection of a simple hinged control surface, defining the law expressing the optimal angle of deflection law as a function of the lift coefficient, the pitching moment variation, the trim effect, and the wave drag effect. In this article, a multi-hinge system is introduced, deriving its capability in enhancing the reference aircraft general performance. To address the aerodynamic analyses on the target morphing airfoil, the concept architecture is described in section "Morphing airfoil structural concept." A 2D sensitivity analysis performed to evaluate the upgrade of the characteristic coefficients is given in section "Airfoil parameterization and 2D aerodynamic analysis." A parabolic morphing trailing edge formulation was presented, emphasizing some technological issues related to morphing shapes. In section "Aircraft morphing application," the 2D results used to evaluate the general capability improvements on a HALE aircraft are presented. Finally, the conclusions summarize the work steps that were carried out and the overall benefits, achieved on the targeted HALE aircraft.

Morphing airfoil structural concept

To drive aerodynamic investigations toward feasible structural solutions, a morphable architecture was preliminarily identified for the trailing edge ribs. A segmented, finger-like layout was considered to physically implement the transition from the baseline airfoil to the target configurations (Pecora et al., 2016a, 2016b; Figure 1). At each section, the rib was assumed to be partitioned into four consecutive blocks (namely, B0, B1, B2, and B3) hinged to each other along the camber line at stations A, B, and C (Figure 1). The block B0 was rigidly connected to the rest of the wing structure through the rear spar, while all the others were free to rotate around the hinges. In this way, an articulated chain of consecutive segments was realized. Further rod elements (L1 and L2), hinged to non-adjacent blocks, forced the camber line segments to rotate according to specific gear ratios, giving rise to a single-degree-of-freedom (SDOF) mechanical system: if the rotation of any

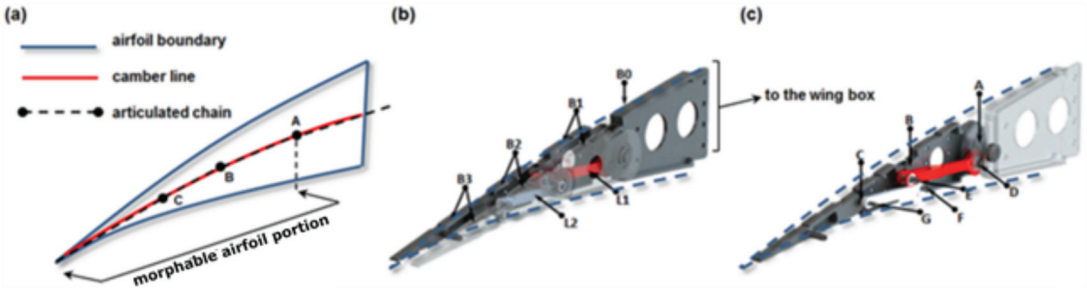

Figure 1. (a) Trailing edge airfoil and morphing rib architecture (blocks and links (b), hinges (c)).

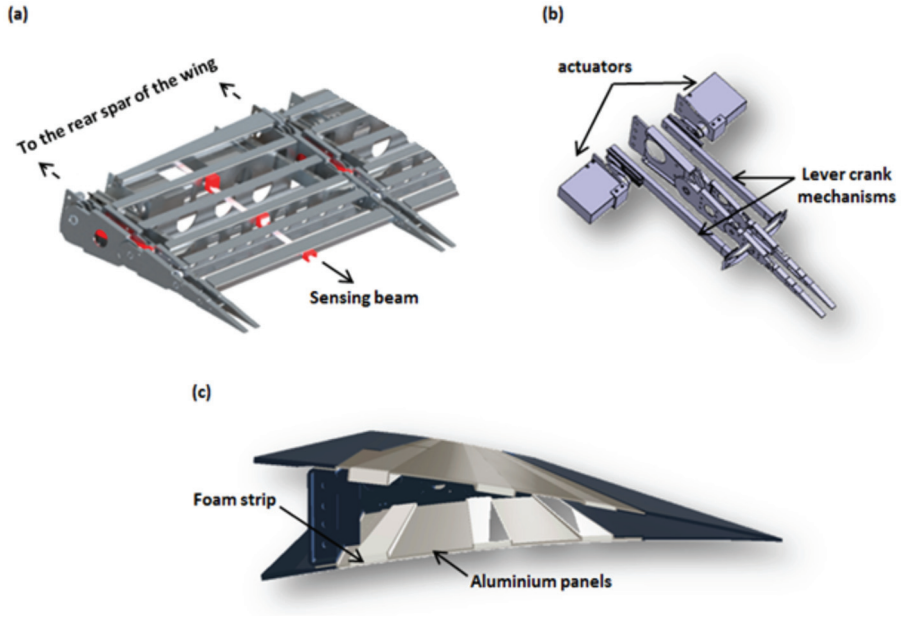

Figure 2. Trailing edge bay: (a) general architecture, (b) actuation system, and (c) compliant skin.

block was prevented, the architecture was fully constrained. On the other hand, if any block was moved from its initial configuration, all the other elements would have followed the motion according to specific ratios.

The ribs' kinematic was transferred to the overall trailing edge structure by means of a multi-box arrangement (Figure 2(a)). Each box of the structural arrangement was assumed to be characterized by a single-cell configuration delimited along the span by homolog blocks of consecutive ribs, and along the chord by longitudinal stiffening elements (spars and/or stringers).

The SDOF mechanism implemented for the ribs and consequently for the multi-box arrangement was suppressed or activated by the actuation system. Servo rotary load-bearing actuators coupled to quick-return mechanisms (Figure 2(b)) were adopted for the independent control of each rib of the device (Amendola et al., 2016; Dimino et al., 2016a, 2016b).

Actuators then played a twofold function: they could lock the blocks' rotation to maintain a given airfoil shape and, at the occurrence, they enabled morphing through a controlled release of the rib kinematics. In both cases, actuators significantly participated in the absorption of the acting loads, pertinent to the airfoil shape being implemented (Dimino et al., 2014).

A fiber Bragg grating (FBG)–based system based on sensing elastic beams located at the middle of each bay was used to detect shape configurations and to generate the information for appropriate open- and closed-loop control actions.

A multi-material arrangement (Schorsch et al., 2015) was finally assumed for the upper and lower skin (Figure 2(c)): more in detail, a rational combination of Al-alloy panels and soft foam strips was implemented along the chord-wise direction. Foam strips were placed in correspondence with camber line hinges, thus adsorbing the tension and compression induced by the camber morphing on the skin; aluminum panels were riveted along rib edges to increase the torsional stiffness of each adaptive trailing edge device (ATED) box. Silicone material—properly designed to withstand

Table 1. NASA LRN 1015 characteristics.

Maximum thickness $(t/c)_{max}$	15.2%c
Position in chord of $(t/c)_{max}$	40%c
Maximum camber δ_{max}	4.9%c
Position in chord of δ_{max}	44%c
Design lift coefficient c_{li}	1.0

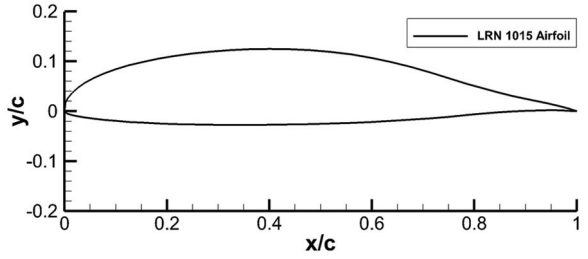

Figure 3. NASA LRN 1015 airfoil.

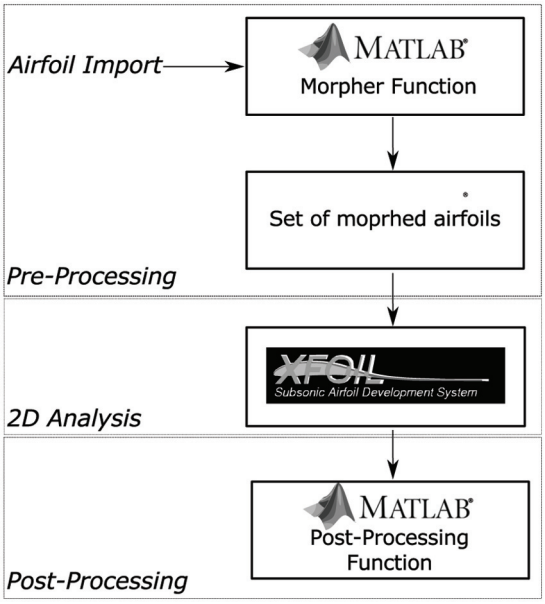

Figure 4. Morphing airfoil 2D analysis: flowchart.

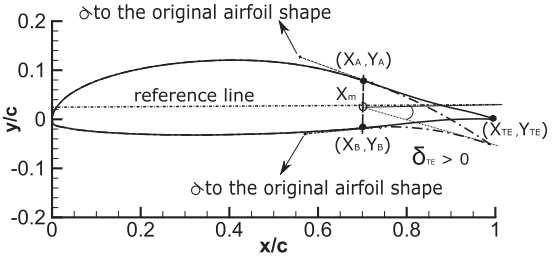

Figure 5. Scheme of the trailing edge morphing.

temperature excursion typically expected in flight—was introduced as the protective layer and glued on the sequence of aluminum panels and foam strips.

The structural concept herein described is extremely versatile to enable shape transitions based on camber line modifications at constant thickness distribution. The number of blocks and their chord-wise extension were defined to satisfactorily match the specified form envelope, from the baseline to the deformed configurations, while avoiding complicating the structural system too much. In fact, a larger number of smaller blocks would have surely assured a more accurate reproduction of the specified outlines. Nevertheless, it would have had considerable impacts on the feasibility of the arrangement as well as on the manufacturing and maintenance costs, because of the high number of parts. Conversely, a smaller number of larger blocks would have led to very simple layouts but would have probably resulted inadequate to adequately reproduce prescribed shapes. The right solution was clearly identified in a proper balance between the needs and the requirements, of course suitable with the specific addressed problem. Previous studies (Pecora et al., 2014) demonstrated that three blocks were sufficient to assure a good level reproduction of the target configurations without significant increase in the system complexity and weight. In detail, nearly 20% weight increase was estimated with respect to conventional wing trailing edge structures, on the basis of calculations applicable to large aspect ratio wings (Peter et al., 2015).

Airfoil parameterization and 2D aerodynamic analysis

The chosen airfoil was the NASA LRN 1015, as shown in Figure 3. The first two digits following the acronym LRN indicate the design lift coefficient in tenths, while the last two digits indicate the maximum camber location in hundredths of chord. The design lift coefficient is then 1.0; the maximum thickness is 15.2%, located at the 40% of the chord, while the maximum camber is 4.9%, located at the 44% of the chord. These characteristics are summarized in Table 1.

To investigate the aerodynamic behavior of the reference airfoil with a morphing trailing edge, a simple parabolic discrete parametrization of its geometry was assumed, in full compliance with the adaptive structural system that was previously described. A rapid tool for the design and analysis of morphing airfoils was set up, according to the block diagram shown in Figure 4. According to that logic, the process started with a preprocessing phase: a reference geometry was imported into a "morpher" function developed in MATLAB®. The user could then define two design parameters, that is, the starting point of the morphing occurrence (X_m) and the rotation angle of the trailing edge (δ_{TE}; Figure 5). Alternatively, he could assign a range of variation for the same variables. At that point, the

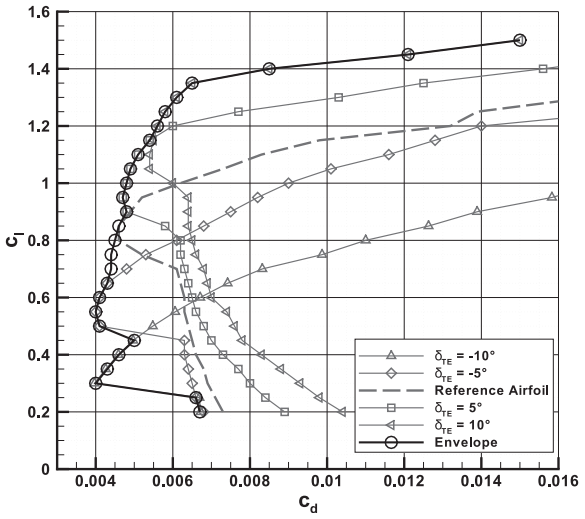

Figure 6. Example of 2D Xfoil analysis: minimum drag envelope at fixed X_m = 0.80, Re = $3e^6$, and M = 0.20.

Table 2. NASA LRN 1015 morphing trailing edge parameters and aerodynamic conditions.

Reference airfoil	NASA LRN 1015
δ_{TE} (°)	[−10:1, + 10]
X_m (x/c)	[0.70, 0.05, 0.95]
Reynolds number	$3e^6$
Mach number	0.2
Flow transition	Free
Critical n parameter	9

LRN: low Reynolds number.

morpher function generated N × M number of morphed airfoils (number of possible starting morphing occurrences × the number of desired rotations). For each morphed airfoil, defined through the starting point of its deformation, an xy text file was generated. Once the pre-processing ended, the input files for the subsequent aerodynamic analyses are generated, that is, the whole set of morphed airfoils. These data are then given as input to the 2D aerodynamic analysis that calls in batch mode the chosen software for the due calculations.

The selected software for the 2D investigation was Xfoil. It was written by Mark Drela at MIT in 1986 (Drela, 1989) and combines high-order panel with fully coupled inviscid/viscous interaction methods. The main reason behind this choice was that it can return results much more quickly than an advanced computational fluid dynamics (CFD) software (like a Navier–Stokes equation solver) in spite of its output being accurate enough to allow a preliminary evaluation of the airfoil aerodynamic characteristics (Lafountain et al., 2009). After the analysis of the generated airfoils' bundle was concluded, a post-processing function elaborated the aerodynamic data to find the δ_{TE} minimizing the drag coefficient c_d at each lift coefficient for a fixed X_m. Then, it found out the value of X_m minimizing the drag among a specified range of variation in the lift coefficient. In this way, the polar envelope is sketched. Together with these parameters, the post-processing function also returned relevant aerodynamic characteristics such as the $C_l^{3/2}/C_d$ variation law, which is fundamental to evaluate the aircraft endurance performance. For better illustrating how the code worked, a reduced number of analyses is illustrated in Figure 6. Therein, the results were obtained by fixing X_m equal to 0.80 and by analyzing four trailing edge deflections: −10°, −5°, + 5°, and + 10°, excluding the baseline. The envelope was obtained by individuating the trailing edge deflection (δ_{TE}) corresponding to the minimum drag at each lift coefficient (circles in Figure 6).

Airfoil trailing edge morphing parameterization

The shape parametrization started with the assignment of the airfoil chord portion (X_m) that would have been affected by the morphing process and the deflection angle (δ_{TE}, positive clockwise). This latter is defined as the rigid rotation of the trailing edge chord with respect to its root. Then both upper and lower coordinates were split into two regions: coordinates that lay before X_m would have not been modified, while the ones that lay behind X_m would have undergone a shape modification, regulated by parabolic functions. The analytical equation of a parabola ($y_{u/l}$) requires three coefficients to be defined; therefore, three equations are needed to determine them. The conditions that were imposed to find the requested parameters are as follows

$$\begin{cases} (X_{TE}, Y_{TE})_{rotated} \in y_{u/l} = a_{u/l}x^2 + b_{u/l}x + c_{u/l} \\ (X_{A/B}, Y_{A/B}) \in y_{u/l} = a_{u/l}x^2 + b_{u/l}x + c_{u/l} \\ \left(\frac{dy}{dx}\right)_{(X_{A/B}, Y_{A/B})} = [\text{tg(upper or lower airfoil curve)}]_{(X_{A/B}, Y_{A/B})} \end{cases} \quad (1)$$

The first two lines impose that the parabola passes through the trailing edge tip and the upper or lower point lying on the upper or lower airfoil surface at the root station X_m. Besides, to avoid profile first-order discontinuities, the parabola must be tangential to the original airfoil shape in correspondence of X_m, as shown in Figure 5 and imposed in the last equation of system (1). Such equations permit calculating six parameters (three for the upper and three for the lower surfaces). The process can be synthetically expressed as

$$\begin{Bmatrix} a_{u/l} \\ b_{u/l} \\ c_{u/l} \end{Bmatrix} = \begin{bmatrix} X_{A/B}^2 & X_{A/B} & 1 \\ 2X_A & 1 & 0 \\ X_{TE}^2 & X_{TE} & 0 \end{bmatrix}^{-1} \cdot \begin{Bmatrix} Y_{A/B} \\ b_{u/l} \\ Y_{TE} \end{Bmatrix} \quad (2)$$

The adoption of this simple mathematical formulation for describing a morphing shape of a generic airfoil also regards technological aspects. In fact, a best

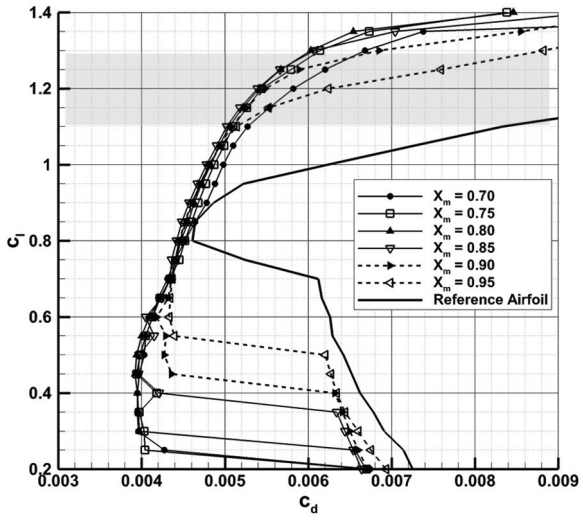

Figure 7. Airfoil drag polar: effect of X_m, M = 0.2 and Re = $3e^6$ on a range of $\delta_{TE} \in [-10, 10]$.

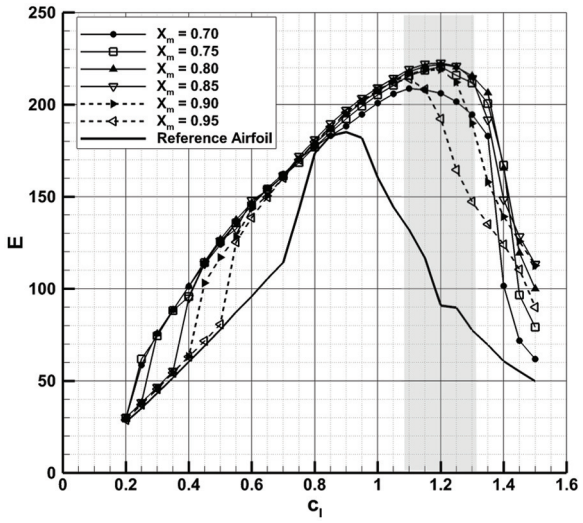

Figure 9. Effect of X_m on aerodynamic efficiency (E), M = 0.2 and Re = $3e^6$ on a range of $\delta_{TE} \in [-10, 10]$.

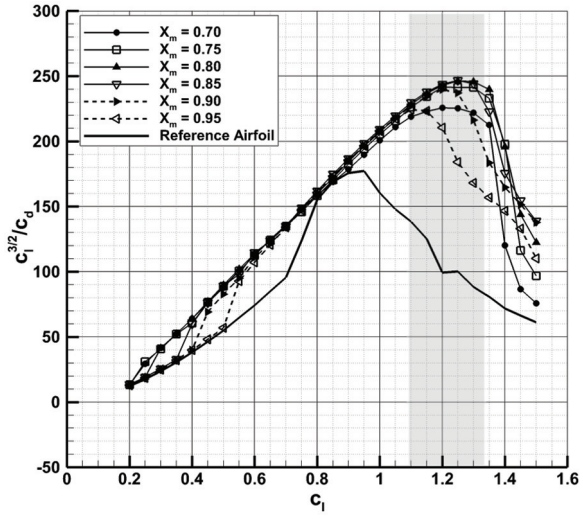

Figure 8. Effect of X_m on $C_l^{3/2}/C_d$, M = 0.2 and Re = $3e^6$ on a range of $\delta_{TE} \in [-10, 10]$.

lift-to-drag ratio could be achieved by combining curvature modifications with chord extensions (as it occurs for typical flap devices). This option is not, however, considered because the adaptive strategy under consideration only allows for curvature adjustments.

2D aerodynamic results

Aerodynamic investigations about the effects of continuously modifying the curvature of the NASA LRN 1015 were then conducted. According to the constraints imposed by the selected morphing technology, X_m was limited within the range of 70%–95% (step 5%) of the airfoil chord, while δ_{TE} was limited within the range between $-10°$ and $10°$ (step $1°$). The aerodynamic analysis was conducted at $3e^6$ Re and 0.20 M, representative of loiter flight condition for a long-endurance UAV. Tested conditions are summarized in Table 2. From Figures 7 to 9, the effect of X_m is shown, with reference to the impacts over the polar, the parameter $C_l^{3/2}/C_d$, and the aerodynamic efficiency. The results are parameterized in X_m while the points on each curve are obtained at the δ_{TE} angle that minimizes the drag at each lift coefficient. In the pictures, the lift coefficient range of 1.1–1.3 is highlighted; in this range, the morphed airfoil exhibits the maximum value of $C_l^{3/2}/C_d$, while the reference airfoil has its maximum ratio $C_l^{3/2}/C_d$ at a lift coefficient around 1, as it is shown in Figure 9. Therein, the optimal reduction in the drag coefficient (20–120 drag counts) can be obtained at $X_m = 0.80$, corresponding to about 40% increment of the $C_l^{3/2}/C_d$ ratio. Figure 10 shows the required trailing edge rotation with respect to the lift coefficient to achieve the best drag reduction and the related maximum increment of the aerodynamic efficiency. As it is clearly outlined in Figure 11, the gain in terms of drag is due to the possibility of reaching a specific c_l by morphing the trailing edge instead of increasing the angle of attack, classically. This aspect directly affects the extension of the laminar flow on the airfoil surface. Figure 12 illustrates how the laminar flow region on the upper surface of the morphing airfoil is larger than the reference one, in the selected lift coefficient range. It is worth to mention that the laminar flow on the lower surface of the morphing airfoil reduces with respect to the reference one; however, this occurrence has a minor effect than the previous (Figure 13). A morphing trailing edge does not offer advantages in terms of the aerodynamic characteristics, only. As a matter of fact, it leads to a relevant increase in the pitching moment coefficient (similar to a classical flap

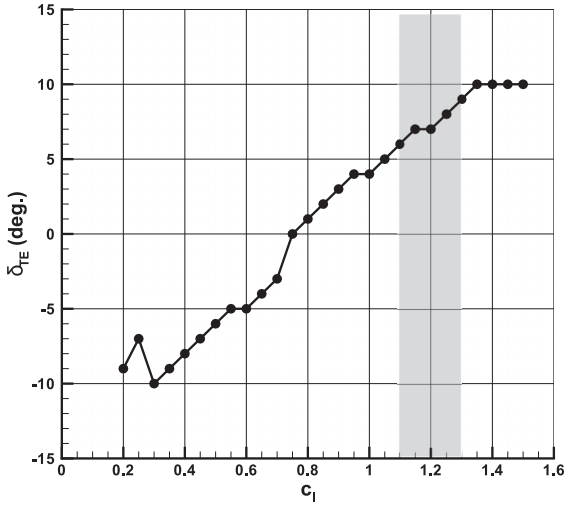

Figure 10. Required trailing edge deflection for the best morphed airfoil envelope, M = 0.2 and Re = $3e^6$.

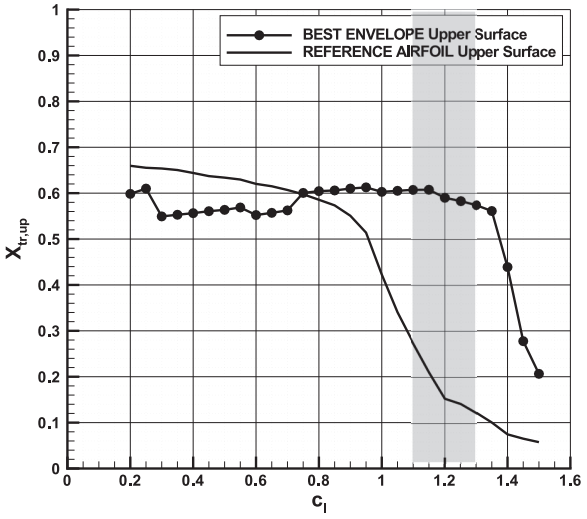

Figure 12. Best envelope morphed airfoil transition abscissa on airfoil upper surface ($X_{tr,up}$) versus c_l, M = 0.2 and Re = $3e^6$.

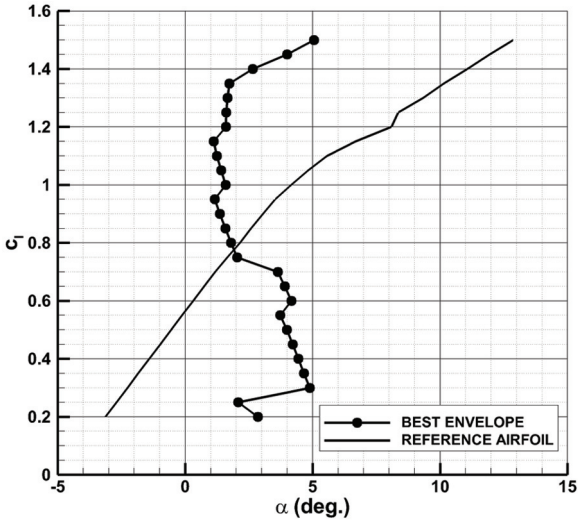

Figure 11. Best envelope morphed airfoil c_l versus α, M = 0.2 and Re = $3e^6$.

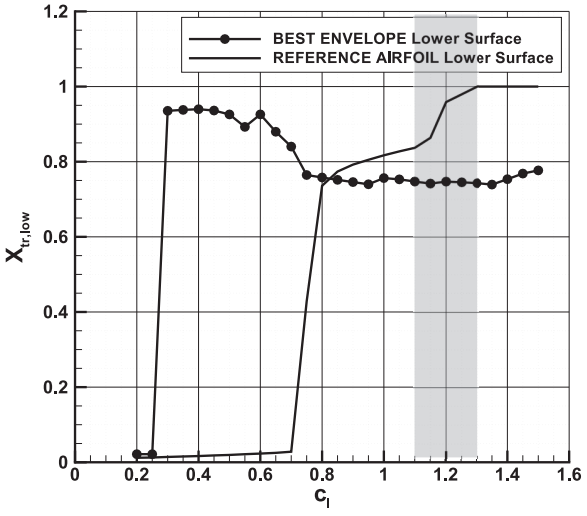

Figure 13. Best envelope morphed airfoil transition abscissa on airfoil lower surface $X_{tr,low}$ versus c_l, M = 0.2 and Re = $3e^6$.

deflection). Figure 14 shows how, in the selected range of lift, the value of this factor for the morphing airfoil is doubled with respect to the reference one. This fact affects the calculation of the parameters of the complete aircraft.

Aircraft morphing application

Starting from the achieved results, the effects of the application of the trailing edge morphing technology on a HALE aircraft were then faced. Such a plane is designed to have a long endurance (30–40 h, Naftel, 2007) or, alternately, a long range. Its performance can be evaluated according to the Breguet equations for a propeller

$$\begin{aligned} R &= \frac{\eta}{SFC}\frac{L}{D}\ln\frac{W_0}{W_1} \\ En &= \frac{\eta}{SFC}\frac{C_L^{3/2}}{C_D}\sqrt{2\rho_\infty S_W}\left(\frac{1}{\sqrt{W_1}}-\frac{1}{\sqrt{W_0}}\right) \end{aligned} \tag{3}$$

In the above equation, R is the range and En is the endurance. The reference aircraft used to perform this evaluation exhibited the typical layout of long-endurance vehicles with lifting surfaces similar to the Global Hawk ones (Naftel, 2007). The reference design is a propeller-driven aircraft unlike the Global Hawk that uses jets.

Figure 15 shows its upper view. The aircraft had an aspect ratio of 25 with a reference area of about 33 m^2, a slender fuselage of 13 m long, and a maximum

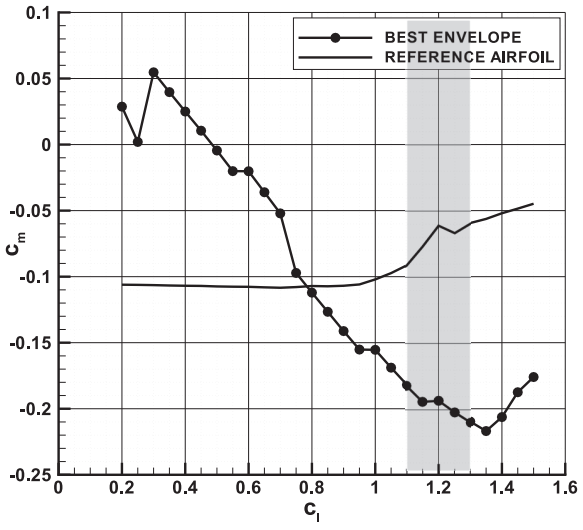

Figure 14. Best envelope morphed airfoil c_m versus c_l, M = 0.2 and Re = $3e^6$.

diameter of about 2 m. The ratios of both the horizontal and the vertical tail with respect to the wing area (S_h/S_w and S_v/S_w) were about 0.18. The maximum take-off weight (MTOW) and the maximum usable fuel mass were, respectively, about 10,000 and 5000 kg, respectively. The aircraft is a twin-engine turboprop having a maximum available thrust of 12,750 N × 2 and a specific fuel consumption of about 330 lb/h. These main characteristics are summarized in Table 3.

The evaluation of the aircraft performance was accomplished through classical approaches like those suggested by Roskam and Lan (1997). The calculation requires the estimation of the aircraft drag polar. For the application proposed in this article, the drag polar was estimated as shown in equation (4)

$$C_{D_{AC}} = \underbrace{C_{D_0}(\text{fus.} + \text{tail} + \text{nac.} + \text{misc.})}_{\text{Parasite drag}} + \underbrace{\Delta C_{D_{F+N}}(\alpha)}_{\text{Fus.} + \text{Nac.parasite drag f}(\alpha)} + \underbrace{C_{D_W}(\alpha)}_{\text{Wing parasite drag f}(\alpha)} + \underbrace{\frac{(C_L^2 - C_{L_0}{}^2)}{\pi AR} \cdot (1 + \delta)}_{\text{Vortex drag}} + \Delta C_{D_{Trim}} \quad (4)$$

where the complete aircraft drag coefficient, $C_{D_{AC}}$, is the summation of the parasite drag without wing, C_{D_0}, a part linked to the fuselage and the nacelles due to the angle of attack variation, $\Delta C_{D_{F+N}}(\alpha)$, the wing parasite drag coefficient, $C_{D_W}(\alpha)$, the vortex drag contribution, and the trim drag, $\Delta C_{D_{Trim}}$. The zero-lift drag coefficient was estimated as suggested by Kroo (2011). This term contains the non-lifting skin friction and viscous pressure drag, the fuselage upsweep drag, the control surface gap drag, the nacelles base drag, contributions due to interference effects among the aircraft components, and, finally, other miscellaneous items. The fuselage and nacelles drag coefficient variation depending on the incidence was estimated by applying the method suggested by Wolowicz and Yancey (1972). It depends on the geometric characteristics of an equivalent body of revolution having the same maximum cross-sectional area, volume, and fineness ratio. The vortex drag contribution was computed according to the typical parabolic drag polar approximation, assuming a difference value for the induced drag factor, δ, taking into account the different wing lift distribution for the un-morphed and the morphed wing. This term was assumed, respectively, equal to 0.04 and 0.07 by computing the wing span lift distribution according to the Multhopp method (Multhopp, 1950). The trim drag, due to the lift force produced by the horizontal tail plane to trim the pitching moment of the wing–fuselage combination, was calculated according to equation (5) (Roskam and Lan, 1997)

$$\Delta C_{D_{Trim}} = \frac{(\Delta C_{L_H})^2}{\pi AR_H e_H} \frac{\bar{q}_H}{\bar{q}} \frac{S_H}{S_W} \quad (5)$$

ΔC_{L_H} is the tail lift coefficient required to trim the aircraft; $\bar{q}$ and $\bar{q}_H$ are the dynamic pressures of the free stream and the one acting on the tail, respectively; AR_H and e_H are the tail aspect ratio and the tail-induced drag factor, respectively, in the order. ΔC_{L_H} is directly related to the non-trimmed pitching moment coefficient of the complete aircraft and the horizontal tail volumetric ratio V_H, according to equation (6)

$$\Delta C_{L_H} = \frac{C_{M_{c.g.}}}{V_H} \quad (6)$$

Table 3. Reference aircraft characteristics.

Reference aircraft type HALE UAV			
Wing AR	25	MTOW	10,000 kg
Wing reference area (S_w)	33 m^2	MF	5000 kg
Fuselage length (l_F)	13 m	Maximum thrust of one engine (To)	12,750 N
Fuselage maximum diameter (d_F)	2.0 m	SFC	150 kg/h
S_h/S_w	0.18	S_v/S	0.18

HALE: high-altitude long-endurance; UAV: unmanned aircraft vehicle; AR: aspect ratio; MTOW: maximum take-off weight; MF: maximum fuel mass; SFC: specific fuel consumption.

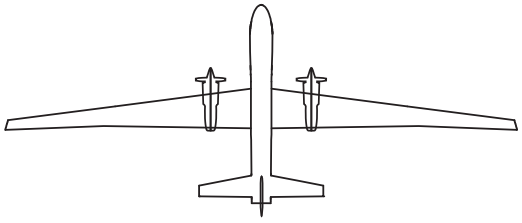

Figure 15. Reference aircraft for the morphing application: upper view.

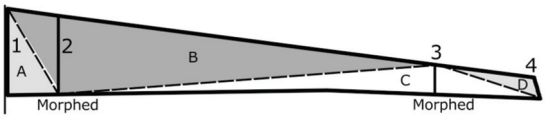

Figure 16. Weighted average Roskam method: scheme for the reference wing with a morphing trailing edge.

More details should be provided about the wing parasite drag contribution, since this term contains the direct effects of the morphing trailing edge. This parameter was calculated as a weighted average of the wing sections' drag characteristics by applying the so-called "influence area method." It allows calculating a generic wing aerodynamic characteristic as an average value of several sections. The procedure consists of splitting the wing into four sections, as illustrated in Figure 16. Sections 2 and 3 were considered to host a morphing airfoil.

A generic three-dimensional (3D) aerodynamic coefficient, C_K, can then be calculated according to equation (7)

$$C_K = K_A \cdot c_{K_1} + K_B \cdot c_{K_2} + K_C \cdot c_{K_3} + K_D \cdot c_{K_4} \quad (7)$$

where K_A, K_B, K_C, and K_D are the ratios between the related areas and the semi-wing surface, while the term c_{K_i} represents the generic 2D aerodynamic coefficient of the standard or the morphed airfoil, according to the considered section

The computation for the case of an un-morphed wing is simplified since only two sections must be considered (1 and 4). The calculation of the lift, drag, and pitching moment coefficients of the reference wing for both morphed and un-morphed configurations was then carried out. The wing 3D aerodynamic characteristics were finally added to the contributions arising from all the other aircraft components. In this way, the complete aircraft could be described in terms of drag polar and pitching moment curve.

Complete aircraft results

The assessed formulation allowed exploiting the 2D results to estimate the complete aircraft performance in terms of drag polar and efficiency. The used morphing parameters and the aerodynamic conditions that were considered to elaborate this analysis are reported in Table 4. The section of the wing, interested by the morphing trailing edge, extended from 10% to 80% span, granting the required space for the deployment of an aileron at the wing tip.

Table 4. Morphing parameters and conditions for the reference aircraft.

Reference airfoil	NASA LRN 1015
Morphed inboard station η_i	0.10
Morphed outboard station η_o	0.80
X_m	0.80
δ_{TE} (°)	[−10:1, + 10]
Reynolds number (Re)	$3e^6$
Mach number (M)	0.20
Loiter altitude	6000 m
MTOW un-morphed	10,000 kg
MTOW morphed	10,240 kg
Center of gravity x/c	0.25
Center of gravity z/c	.00

LRN: low Reynolds number; MTOW: maximum take-off weight.

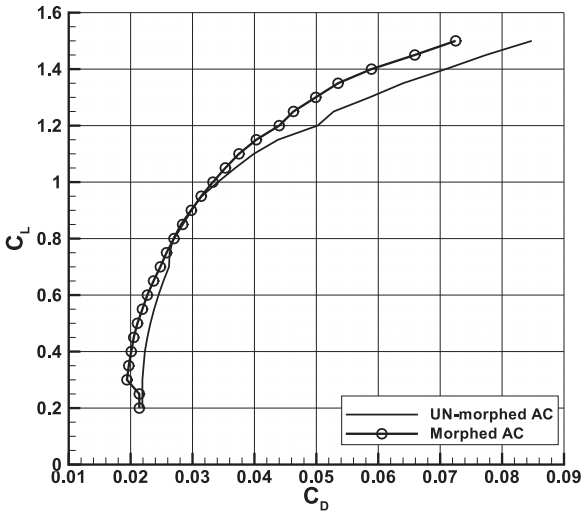

Figure 17. Reference aircraft C_D versus C_L: un-morphed versus morphed.

Figure 17 displays the comparison between the drag polar of the morphed and the un-morphed reference aircraft. The reduction in the drag coefficient, in the range of high C_L, ranges from 10 to more than 100 drag counts. According to Figure 18, the lift coefficient corresponding to the maximum ratio $C_L^{3/2}/C_D$ (representative of the maximum endurance capability) can be estimated to be about 0.95 or 1.3 for the un-morphing and the morphing configurations, respectively. These values lead to different aircraft speeds for maximum endurance configuration. $C_L^{3/2}/C_D$ shifts from about 29 to 34, evidence of a better endurance performance.

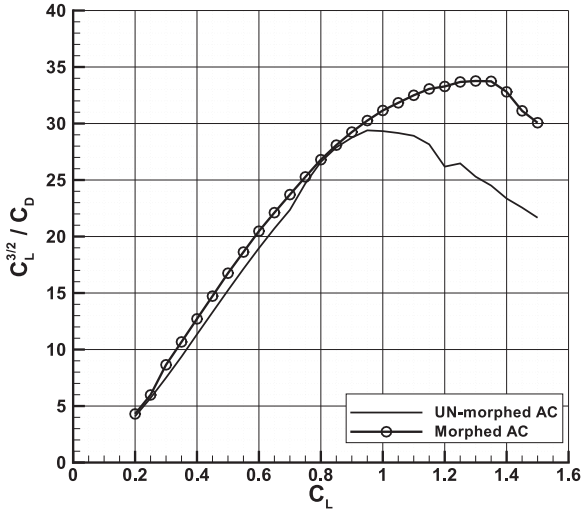

Figure 18. Reference aircraft $C_L^{3/2}/C_D$ versus C_L: un-morphed versus morphed.

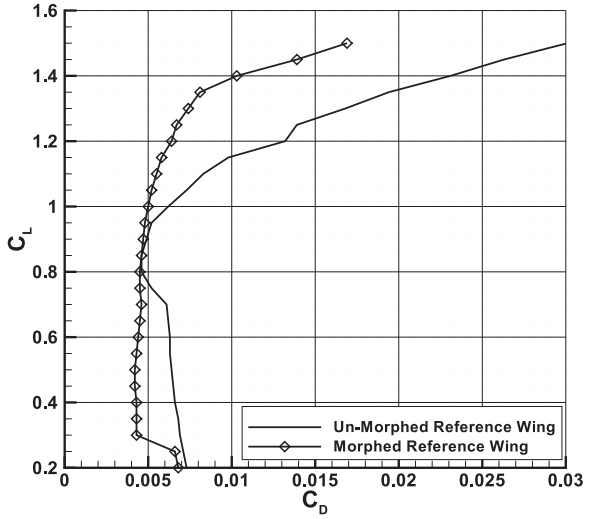

Figure 20. Reference wing drag polar: un-morphed versus morphed.

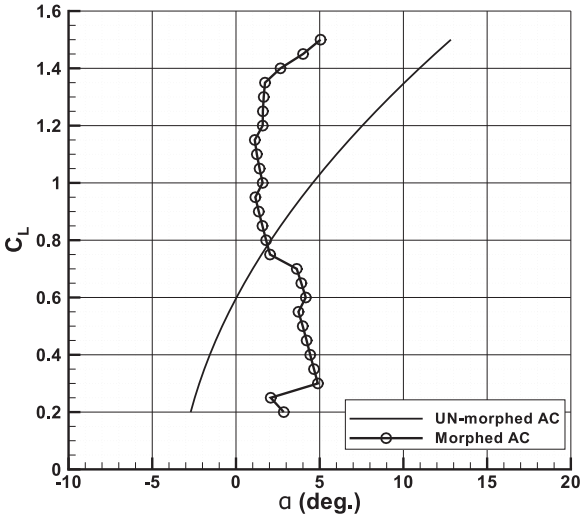

Figure 19. Reference aircraft C_L versus α: un-morphed versus morphed.

Figure 19 shows the lift curve for both configurations. The un-morphed aircraft needs an angle of attack of about 7° to reach the optimal C_L while the morphing system requires an incidence of just 2°–3°. The drag reduction, the gain of efficiency, and the increment of $C_L^{3/2}/C_D$ are primarily due to the change in the wing aerodynamic characteristics, as clearly outlined by comparing the wing drag polar (Figure 20). In the complete aircraft configuration, the fuselage effect must be considered. Because the morphed and un-morphed configurations reach the maximum ratio $C_L^{3/2}/C_D$ at different incidences, the fuselage works differently. Moving from 7° to 2°–3°, a gain of about 1%–2% is predicted.

Aircraft morphing configuration leads to lower fuselage attitude, a lower fuselage pitching moment contribution, and an increment of the wing pitching moment. Globally, the trim drag contribution for both configurations was estimated to be lower than 2% of the total drag at the configuration for the maximum endurance performance, with about one to four drag counts penalty for the morphing aircraft. The drag breakdown for un-morphed and morphed aircraft in the lift coefficient mission range is summarized in Table 5.

In Table 6, a summary of the main aerodynamic characteristics and the flight performance of the morphing and un-morphing aircraft is reported. The use of a morphing trailing edge technology increases the endurance by more than 14%, while maintaining the same range, approximately. This result confirmed the great potential benefits associated with the use of a morphing trailing edge for HALE aircraft.

Further considerations can be deduced. As already discussed in the introduction, HALE aircraft are designed to accomplish missions involving observation, surveillance, survey, monitoring, and so on. In addition to the increased endurance performance, the morphing technology also allows reducing the operational speeds, granting lower speed operations that could be favorable to those targets. The morphing technology could also be used to improve the take-off and landing performance of the aircraft. As a matter of fact, the morphing trailing edge could be used as a plain flap. Assuming a maximum trailing edge deflection equal to + 10° and assuming the possibility of the morphing aircraft to deflect the whole adaptive wing section for that amount at take-off, a 1.94 lift coefficient could be achieved. The un-morphing configuration is characterized by a maximum lift coefficient of about 1.65 (18% lower; Table 6). This result leads to a reduction in the take-off and landing distance of about 16% and 43%,

Table 5. Drag coefficient breakdown for un-morphed (top) and morphed (bottom) aircraft.

C_L	$C_{D\ WING}$	$C_{D\ FUSELAGE}$	$C_{D\ TRIM}$	$C_{D\ TAIL}$	$C_{D\ MISC}$	$C_{D\ VORTEX}$	$C_{D\ TOT}$
Un-morphed (alpha = variable)							
0.8	0.00460	0.00608	0.00006	0.00373	0.00294	0.00847	0.02587
0.9	0.00490	0.00639	0.00008			0.01073	0.02876
1	0.00620	0.00693	0.00010			0.01324	0.03313
1.1	0.00830	0.00785	0.00012			0.01602	0.03896
1.2	0.01320	0.01022	0.00015			0.01907	0.04930
1.3	0.01680	0.01173	0.00020			0.02238	0.05777
1.4	0.02310	0.01419	0.00026			0.02595	0.07017
Morphed (alpha = constant)							
0.8	0.00450	0.00577	0.00005	0.00373	0.00294	0.00872	0.02570
0.9	0.00470	0.00577	0.00011			0.01104	0.02828
1	0.00500	0.00577	0.00020			0.01362	0.03126
1.1	0.00550	0.00577	0.00030			0.01648	0.03472
1.2	0.00640	0.00577	0.00043			0.01962	0.03888
1.3	0.00740	0.00577	0.00057			0.02302	0.04343
1.4	0.01030	0.00577	0.00075			0.02670	0.05019

Table 6. Flight performance of the reference aircraft: morphed versus un-morphed.

Parameter	Un-morphed	Morphed	$\Delta_{Morphing}$
$(C_L^{3/2}/C_D)_{MAX}$	29.43	33.73	+ 14.6%
C_L at $(C_L^{3/2}/C_D)_{MAX}$	0.95	1.3	+ 36%
α at $(C_L^{3/2}/C_D)_{MAX}$	7°	2°/3°	−4°/−5°
En at $(C_L^{3/2}/C_D)_{MAX}$	36 h 21 min	41 h 40 min	+ 14.6%
En at C_L = 1.0	36 h 2 min	38 h 9 min	+ 6%
R at E_{max}	14,743 km	14,793 km	+ 0.3%
$C_{L,MAX}$ (take-off)	1.65	1.94	+ 18%
V_{Stall}	54.3 m/s	50.2 m/s	−8%
Take-off field length	1370 m	1180 m	−16%
Landing field length	1400 m	980 m	−43%

respectively, calculated as suggested by Roskam and Lan (1997).

The installation of the morphing technology brings a weight penalty of about 2% for the morphed configuration with respect to the complete aircraft. To evaluate the weight increment effect, a performance sensitivity analysis has been performed varying the aircraft MTOW for the morphed aircraft (due to the morphed wing trailing edge), keeping it constant for the un-morphed aircraft. The results show a breakeven point of about 9% and 2% of MTOW increment for the endurance and range performance, respectively, as shown in Figures 21 and 22.

Conclusion

The application of a morphing trailing edge on a HALE aircraft was performed, showing promising improvement for both in-flight and on-ground performance. The feasibility of this device was largely demonstrated in the literature and it could be compliant with a real aircraft specification. A systematic parametric aerodynamic analysis, conducted on a typical HALE aircraft airfoil, showed that a morphing trailing edge extension of 20% along the airfoil chord with a deflection capability of $\pm 10°$ is the best compromise between the expected performance improvement and the architectural complication. The benefits may be calculated to approach a 30% improvement in terms of maximum efficiency in the climb rate, while reducing the drag coefficient in a wide range of lift coefficients. This latter effect derives from the capability of controlling the airfoil boundary layer and the transition, mainly. Such a device can improve the endurance of about 15% (more than 4 h) while keeping the same range. Ground performance is improved in terms of take-off and landing runs of about 15% and 40%, respectively. The weight penalty, associated with the introduction of a morphing trailing edge system on board of the target aircraft, is estimated to be 2% of its

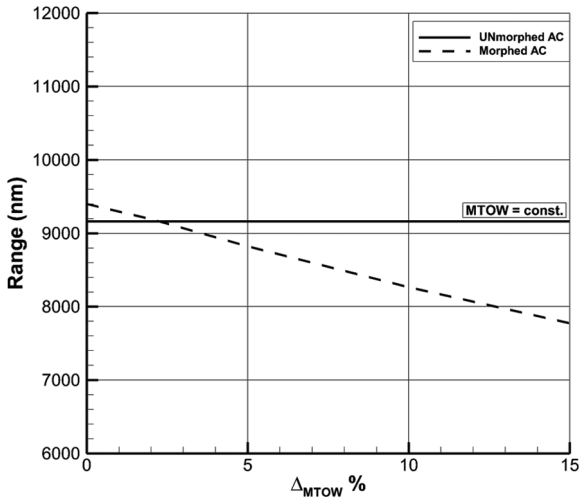

Figure 21. Weight increment effect (due to morphing) on the aircraft range.

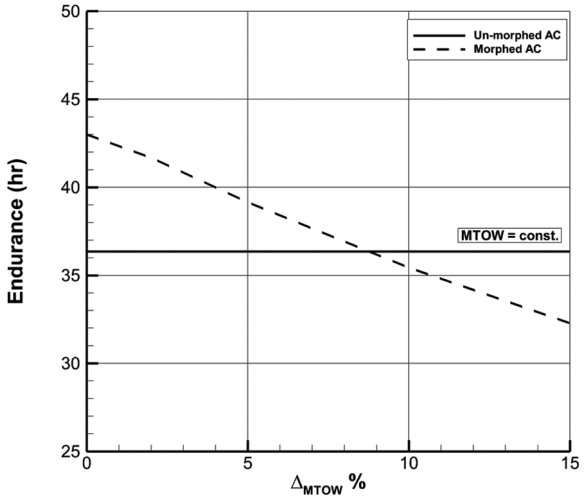

Figure 22. Weight increment effect (due to morphing) on the aircraft endurance.

MTOW, and the breakeven point has been evaluated to be around 9% for the endurance performance and 2% for aircraft range.

Keeping in mind these preliminary results, the detailed design of a wing hosting a morphing trailing edge will be prepared. Wing loads will be accurately estimated to define the critical loads to properly size the wing structure and the adaptive system. Further works will deal with the investigations of the possible application of differential span-wise morphing devices to augment the aircraft aerodynamic controllability.

Declaration of conflicting interests

The author(s) declared no potential conflicts of interest with respect to the research, authorship, and/or publication of this article.

Funding

The author(s) received no financial support for the research, authorship, and/or publication of this article.

References

Ajaj RM, Beaverstock CS and Friswell MI (2016) Morphing aircraft: the need for a new design philosophy. *Aerospace Science and Technology* 49: 154–166.

Amendola G, Magnifico M, Pecora R, et al. (2016) Distributed actuation concepts for a morphing aileron device. *The Aeronautical Journal* 120(1231): 1365–1385.

Barbarino S, Bilgen O, Ajaj RM, et al. (2011) A review of morphing aircraft. *Journal of Intelligent Material Systems and Structures* 22(9): 823–877.

Bolonkin A and Gilyard GB (1999) *Estimate benefits of variable-geometry wing camber control for transport aircraft*. NASA technical memorandum no. 1999-206586. Edwards, CA: Dryden Flight Research Center.

Bowman J, Sanders B, Cannon B, et al. (2007) Development of next generation morphing aircraft structures. In: *48th AIAA/ASME/ASCE/AHS/ASC structures, structural dynamics, and materials conference*, Honolulu, HI, 23–26 April. Reston, VA: American Institute of Aeronautics and Astronautics.

Chang IC, Torres FJ and Tung C (1995) *Geometric analysis of wing sections*. NASA technical memorandum no. 110346, April. Moffett Field, CA: Ames Research Center.

De Gaspari A and Ricci S (2010) Combining shape and structural optimization for the design of morphing airfoils. In: *2nd international conference on engineering optimization*, Lisbon, 6–9 September.

Della Vecchia P (2013) *Development of methodologies for the aerodynamic design and optimization of new regional turboprop aircraft*. PhD Thesis, University of Naples Federico II, Naples.

Della Vecchia P, Daniele E and D'Amato E (2014) An airfoil shape optimization technique coupling PARSEC parameterization and evolutionary algorithm. *Aerospace Science and Technology* 32(1): 103–110.

Derksen RW and Rogalsky T (2010) Bezier-PARSEC: an optimized aerofoil parameterization for design. *Advances in Engineering Software* 41(7–8): 923–930.

Dimino I, Concilio A and Pecora R (2016a) Safety and reliability aspects of an adaptive trailing edge device (ATED). In: *24th AIAA/AHS adaptive structures conference*, San Diego, CA, 4–8 January.

Dimino I, Diodati G, Concilio A, et al. (2016b) Distributed electromechanical actuation system design for a morphing trailing edge wing. In: *Proceedings of the SPIE industrial and commercial applications of smart structures technologies* 2016, 980108, Las Vegas, NV, 20 March, vol. 9801.

Dimino I, Flauto D, Diodati G, et al. (2014) Actuation system design for a morphing wing trailing edge. *Recent Patents on Mechanical Engineering* 7(2): 138–148.

Drela M (1989) An analysis and design system for low Reynolds number airfoils. In: Mueller TJ (ed.) *Lecture Notes in Engineering*, vol. 54. Berlin, Heidelberg: Springer-Verlag, pp. 1–12.

Fincham JS and Friswell MI (2015) Aerodynamic optimisation of a camber morphing aerfoil. *Aerospace Science and Technology* 43: 245–255.

Fudenberg D and Tirole J (1991) *Game Theory*. Boston, MA: Massachusetts Institute of Technology Press.

Gabor OS, Koreanschi A and Botez RM (2016) Numerical simulation and wind tunnel tests investigation and validation of a morphing wing-tip demonstrator aerodynamic performance. *Aerospace Science and Technology* 53: 136–153.

Hicks RM and Cliff SE (1991) *An evaluation of three two-dimensional computational fluid dynamics codes including low Reynolds numbers and transonic Mach numbers*. NASA technical memorandum no. 102840, January. Moffett Field, CA: Ames Research Center.

Hicks RM and Henne PA (1978) Wing design by numerical optimization. *Journal of Aircraft* 15(7): 407–412.

Hicks RM and Vanderplaats GR (1975) *Applications of numerical optimization to the design of low-speed airfoil*. NASA technical memorandum no. X-3213. March. Moffett Field, CA: Ames Research Center.

Kaul U and Nguyen NT (2014) Drag optimization study of variable camber continuous trailing edge flap (VCCTEF) using OVERFLOW. In: *32nd AIAA applied aerodynamics conference, AIAA aviation forum*, Atlanta, GA, 16–20 June. Reston, VA: American Institute of Aeronautics and Astronautics.

Kroo I (2011) *Aircraft Design: Synthesis and Analysis*. Stanford, CA: Stanford University.

Lafountain C, Cohen K and Abdallah S (2009) Camber controlled airfoil design for morphing UAV. In: 4 *7th AIAA aerospace sciences meeting including the new horizons forum and aerospace exposition*, Orlando, FL, 5–8 January. Reston, VA: American Institute of Aeronautics and Astronautics.

Lane K and Marshall D (2009) A surface parameterization method for airfoil optimization and high lift 2D geometries utilizing the CST methodology. In: *47th AIAA aerospace sciences meeting including the new horizons forum and aerospace exposition*, Orlando, FL, 5–8 January. Reston, VA: American Institute of Aeronautics and Astronautics.

Multhopp H (1950) *Methods for calculating the lift distribution of wings (subsonic lifting surfaces theory)*. Aeronautical Research Council reports and memoranda no. 2884, January. London: Ministry of Supply, Royal Aircraft Establishment.

Naftel CJ (2007) *NASA Global Hawk: a unique capability for the pursuit of earth science*. NASA technical memorandum no. 2007-214613, March. Edwards, CA: Dryden Flight Research Center.

Pecora R, Amoroso F, Amendola G, et al. (2014) Validation of a smart structural concept for wing-flap camber morphing. *Smart Structures and Systems* 14(4): 659–678.

Pecora R, Amoroso F, Magnifico M, et al. (2016a) KRISTINA: kinematic rib-based structural system for innovative adaptive trailing edge. In: *Proceedings of the SPIE industrial and commercial applications of smart structures technologies 2016*, 980108, Las Vegas, NV, 20 March, vol. 9801.

Pecora R, Concilio A, Dimino I, et al. (2016b) Structural design of an adaptive wing trailing edge for enhanced cruise performance. In: *24th AIAA/AHS adaptive structures conference*, San Diego, CA, 4–8 January. Reston, VA: American Institute of Aeronautics and Astronautics.

Peter F, Stumpf E, Carossa G, et al. (2015) Morphing value assessment on overall aircraft level (Chapter XI). In: Wölcken PC and Papadopoulos M (eds) *Smart Intelligent Aircraft Structures (SARISTU) (Proceedings of the final project conference)*. Berlin, Heidelberg: Springer-Verlag, pp. 859–872.

Ramamoorthy P, Dwarakanath GS and Narayana CL (1969) Wagner functions. Technical report, 22 December. National Aeronautical Laboratory, Bangalore, India.

Raymer D (2006) *Aircraft Design: A Conceptual Approach*. Reston, VA: American Institute of Aeronautics and Astronautics.

Roskam J and Lan CT (1997) *Airplane Aerodynamics and Performance*. Lawrence, KS: Design, Analysis and Research Corporation.

Samareh JA (1999) A survey of shape parameterization techniques. In: *CEAS/AIAA/ICASE/NASA Langley international forum on aeroelasticity and structural dynamics*, Williamsburg, VA, 22–25 June, pp. 333–343. Washington, DC: National Aeronautics and Space Administration.

Schorsch O, Luhring A, Nagel C, et al. (2015) Polymer based morphing skin for adaptive wings. In: *7th ECCOMAS thematic conference on smart structures and materials (SMART)*, Azores, 3–6 June.

Sobieczky H (1997) Geometry generator for CFD and applied aerodynamics. In: Sobieczky H (ed.) *Courses and Lecture International*, vol. 366. Vienna: Springer-Verlag, pp. 137–157.

Sobieczky H (1998) Parametric airfoils and wings. In: Fujii K and Dulikravich GS (eds) *Notes on Numerical Fluid Mechanics*, vol. 68. Wiesbaden: Vieweg, pp. 71–88.

Wenbin S (2011) A naturally bounded parameterization method for airfoil shape optimization. In: *52nd AIAA/ASME/ASCE/AHS/ASC structures, structural dynamics, and materials conference*, Denver, CO, 4–7 April.

Wolowicz CH and Yancey RB (1972) *Longitudinal aerodynamic characteristics of light, twin-engine propeller-driven airplanes*. NASA technical report no. D-6800, June. Washington, DC: National Aeronautics and Space Administration.